




Synthesis, characterization and electrocatalytic behavior of cobalt and iron phthalocyanines bearing chromone or coumarin substituents

Sumayya Chohan, Irvin Noel Booyesen, Allen Mambanda & Matthew Piers Akerman

To cite this article: Sumayya Chohan, Irvin Noel Booyesen, Allen Mambanda & Matthew Piers Akerman (2015) Synthesis, characterization and electrocatalytic behavior of cobalt and iron phthalocyanines bearing chromone or coumarin substituents, Journal of Coordination Chemistry, 68:10, 1829-1846, DOI: [10.1080/00958972.2015.1023196](https://doi.org/10.1080/00958972.2015.1023196)

To link to this article: <http://dx.doi.org/10.1080/00958972.2015.1023196>

 View supplementary material 

 Accepted author version posted online: 25 Feb 2015.
Published online: 24 Mar 2015.

 Submit your article to this journal 

 Article views: 99

 View related articles 

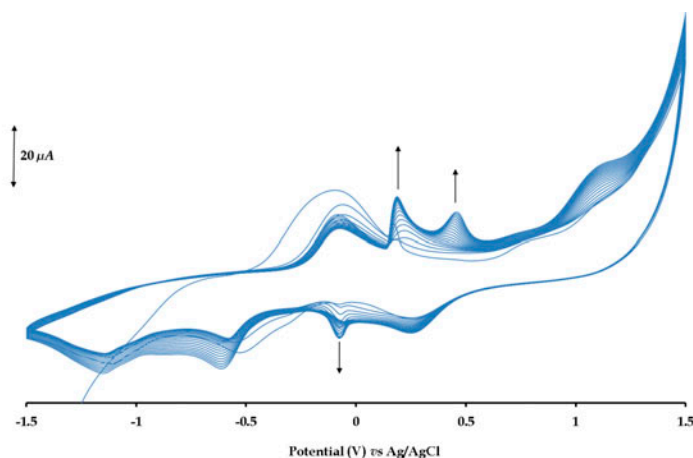
 View Crossmark data 

Synthesis, characterization and electrocatalytic behavior of cobalt and iron phthalocyanines bearing chromone or coumarin substituents

SUMAYYA CHOCHAN, IRVIN NOEL BOOYSEN*, ALLEN MAMBANDA and MATTHEW PIERS AKERMAN

School of Chemistry and Physics, University of Kwazulu-Natal, Pietermaritzburg, South Africa

(Received 24 November 2014; accepted 5 February 2015)



Cobalt and iron phthalocyanines (Pcs) bearing peripherally tetra-substituted chromone (chr) or coumarin (cou) moieties were formulated and characterized by UV–Vis and FTIR spectroscopy, ESI-TOF mass spectrometry, and elemental analysis. The structural elucidations of the ligands, 4-(chromone-7-oxy)phthalonitrile (**1**) and 4-(4-(trifluoromethyl)-coumarin-7-oxy)phthalonitrile (**2**) were complemented by NMR spectroscopy and single crystal X-ray analysis (for **1**). The redox properties of the complexes were investigated via voltammetry and the subsequent voltammetric assignments were corroborated by UV–Vis spectroelectrochemistry. Each metal complex displayed four redox processes of which their Pc ring oxidations are irreversible and the remaining redox couples are quasi-reversible. Utilizing the respective metallophthalocyanines, modified working electrodes were prepared by electropolymerization and their electrocatalytic activities toward nitrite oxidation were explored. All the metal complexes showed an increase in nitrite oxidation currents and a minor decrease in oxidation potentials which is indicative of electrocatalysis. The trend of electrocatalytic activity was found to be as follows: CoPc–chr (**3**) > FePc–cou (**4**) > CoPc–cou (**5**).

Keywords: Metallophthalocyanine; Chromone; Coumarin; Electropolymerization; Electrocatalysis

*Corresponding author. Email: Booysemi@ukzn.ac.za

1. Introduction

Phthalocyanines (Pcs) were originally used as dyes given their characteristic blue–green color [1–4]. Further studies showed that their metal complexes, metallophthalocyanines (MPcs), are versatile compounds with vast applications in areas such as non-linear optics, chemical sensing, photodynamic therapy, and surface modification through formation of Langmuir–Blodgett films [5–7]. MPcs form stable films on electrode surfaces which behave as active catalysts for a myriad of reactions including nitrite oxidation [8–11]. Typically, good electrocatalysts display durability, enhance electrode sensitivity and selectivity as well as lower the redox potential of an analyte [12]. These electrochemical properties can be optimized by meticulous selection of the metal center as well as the substituents and their positions on the Pc ring [13–16].

The use of MPcs covalently linked to biologically significant substituents has been widely employed in electrocatalysis to allow the selective detection of important biological analytes [9, 17, 18]. In this study, MPcs substituted with chromones (1-benzopyran-4-one) and coumarins (1-benzopyran-2-one) were selected as they are oxygen-containing heterocyclic compounds, known as benzopyrones, which occur naturally in plants [19–22]. The biological activities of these heterocyclic compounds are modulated by different substituents to afford a wide range of properties, such as antioxidant [22–24] and anticoagulant activities [25, 26]. By utilizing the redox-active metal centers, cobalt and iron are motivated by their ability to promote faster electron transfer kinetics for the respective modified MPc-working electrodes, which are essential for electrocatalysis [27–29].

Nitrites are important biological molecules used as food preservatives and fertilizers [30, 31]. However, they combine with hemoglobin in the blood preventing oxygen from penetrating the tissues and also react with amines in the stomach to form carcinogenic nitrosamines [32–34]. The detection of nitrite concentrations is thus imperative for food quality assurance and for the determination of water resource contamination by fertilizer run-offs. Spectral analyses, chromatography, and electrochemical methods have been employed for nitrite detection, the latter of which has proved to be the most time- and cost-effective method [32–36]. In this study, we report the synthesis and characterization of peripherally benzopyrone-substituted MPcs containing redox-active Fe(II) and Co(II) metal centers. In addition, we explore the electrocatalytic oxidation of nitrite using electropolymerized MPcs on platinum working electrodes.

2. Experimental

2.1. Materials and methods

4-Nitrophthalonitrile, 7-hydroxychromone, 7-hydroxy-4-trifluoromethyl coumarin, potassium carbonate, cobalt(II) chloride, iron(II) chloride tetrahydrate, 1,8-diazabicyclo[5.4.0]undec-7-ene (DBU), and electrochemical analysis grade tetrabutylammonium tetrafluoroborate (TBABF₄) were purchased from Sigma–Aldrich and used without purification. Organic solvents, sodium sulfate, phosphorus pentoxide (P₂O₅), molecular sieves (4 Å), and silicon dioxide (silica) for column and thin-layer chromatography were purchased from Merck SA. Aluminum oxide (alumina) as a part of a polishing kit was obtained from Metrohm. Dimethylformamide (DMF) used in ligand synthesis, UV–Vis spectral analysis, and

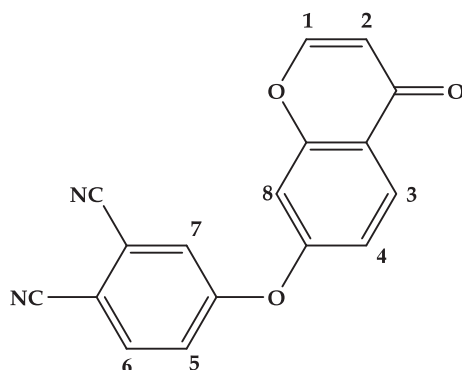
electrochemical experiments was dried and stored over molecular sieves. All metal complexes and ligands were stored over P₂O₅. Ultrapure water was obtained from an Elga Purelab Ultra system.

FTIR spectra were recorded using a Bruker Alpha FT-IR spectrometer equipped with an ATR platinum Diamond 1 reflectance accessory. NMR experiments were conducted in d⁶-DMSO. UV-Vis spectroscopy was carried out using a Perkin-Elmer Spectrum 25. Melting points were recorded using a Stuart SMP3 melting point apparatus. Elemental analysis was carried out using a CHNS-O Flash 2000 Organic Elemental Analyser. Mass spectral analysis of the complexes was done both in the positive and negative modes via the direct injection of the respective samples into the Water Micro-mass LCT Premier LC-MS instrument equipped with an electrospray ionization (ESI) source and a time-of-flight (TOF) mass analyzer. The NMR spectra were collected on a Bruker Avance 400 MHz spectrometer.

Voltammetric studies were conducted using an Autolab Potentiostat equipped with a three-electrode system: a Pt working electrode, a pseudo Ag|AgCl reference electrode, and a Pt counter electrode. The Autolab Nova 1.7 software was used for operating the potentiostat and data analysis. The electrode surface was regenerated between runs by polishing over a slurry of alumina and ultrapure water on a Buehler polishing pad followed by rinsing with ultrapure water and anhydrous DMF. Electrochemical experiments were conducted in deoxygenated solutions of the complexes in DMF containing 0.1 M equivalents of TBABF₄ as a supporting electrolyte. Electropolymerization of the complexes onto a Pt electrode was achieved by repetitive cyclic voltammetry (CV; 20 cycles) in the potential window of -1.5 to +1.5 V. Spectroelectrochemistry experiments were undertaken using a Specac optically transparent thin-layer electrochemical (OTTLE) cell.

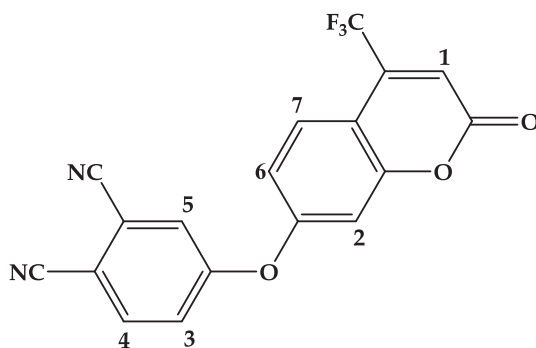
2.2. Synthesis of 4-(chromone-7-oxo)phthalonitrile (**1**)

A mixture of 4-nitrophthalonitrile (1.00 g, 5.78 mM) and 7-hydroxychromone (0.937 g, 5.78 mM) in the presence of a basic catalyst, potassium carbonate (2.30 g, 16.6 mM), was dissolved in anhydrous DMF (30.0 mL). The reaction mixture was heated, while stirring at 90 °C under an inert nitrogen atmosphere for 24 h. The resultant solution was cooled to room temperature and poured into 300 mL of water-ice slurry. The precipitate was filtered and washed with cold ethyl acetate. A light-orange compound was obtained after purification via column chromatography using a 9 : 1 (v : v) ethyl acetate:hexane solvent system. The product was recrystallized by partial slow diffusion of hexane into a solution of **1** in CH₃CN to give yellow-gold, needle-like crystals. Yield: 46%; m.p. (°C): 226.2–226.8; FT-IR ($\nu_{\max}/\text{cm}^{-1}$): $\nu(\text{C}=\text{O})$ 1644, $\nu(\text{C}\equiv\text{N})$ 2231, $\nu(\text{C}-\text{O}-\text{C})$ 1027, 1130; ¹H NMR (ppm): 8.30 (d, 1H, *J* = 6.11 Hz, H1), 6.37 (d, 1H, *J* = 6.23 Hz, H2), 8.12 (d, 1H, *J* = 8.76 Hz, H3), 7.64 (d, 1H, *J* = 8.78 Hz, H4), 7.27 (d, 1H, *J* = 8.79 Hz, H5), 8.18 (d, 1H, *J* = 8.75 Hz, H6), 7.47 (s, 1H, H7), 8.01 (s, 1H, H8); ¹³C NMR (ppm): 176.10, 159.84, 159.16, 157.77, 157.60, 136.91, 128.17, 124.59, 124.42, 121.96, 118.10, 117.43, 116.25, 115.76, 112.90, 110.28, 109.22; UV-Vis (DMF, λ_{\max} (ϵ , M⁻¹ cm⁻¹)): 306 nm (11,010), 295 nm (9962). Molecular mass (*m/z*): Calcd: 288.26. Found: 311.32 [M + Na]⁺. Anal. Calcd for C₁₇H₈N₂O₃ (%): C, 70.83; H, 2.80; N, 9.72. Found: C, 70.19; H, 2.78; N, 9.72.



2.3. Synthesis of 4-(4-(trifluoromethyl)-coumarin-7-oxy)phthalonitrile (2)

Similarly, the reaction of 4-nitrophthalonitrile (1.00 g, 5.78 mM) with 7-hydroxy-4-trifluoromethylcoumarin (1.33 g, 5.78 mM) was initiated in 30 mL of DMF in the presence of K_2CO_3 (2.30 g, 16.6 mM). The reaction mixture was heated with stirring at 90 °C under an inert nitrogen atmosphere for 24 h. Thereafter, the reaction mixture was cooled to room temperature, poured into 60 mL water, and extracted with CH_3CN . The combined organic extracts were dried over sodium sulfate and filtered. The solvent was evaporated under reduced pressure and the remaining residue was added to 30% HCl to induce precipitation. The precipitate was then repeatedly washed with water and added to hot methanol (MeOH), filtered, and dried under P_2O_5 . Yield: 41%; m.p. (°C): 180.0–181.8; FT-IR (ν_{max}/cm^{-1}): $\nu(C=O)$ 1729, $\nu(C\equiv N)$ 2235, $\nu(C-O-C)$ 990, 1129; 1H NMR (ppm): 7.06 (s, 1H, H1), 7.99 (s, 1H, H2), 7.64 (d, 1H, $J = 8.73$ Hz, H3), 8.19 (d, 1H, $J = 8.74$ Hz, H4), 7.43 (s, 1H, H5), 7.28 (d, 1H, $J = 8.80$ Hz, H6), 7.80 (d, 1H, $J = 9.01$ Hz, H7); ^{13}C NMR (ppm): 159.78, 158.74, 158.42, 156.01, 146.85, 137.01, 127.37, 124.64, 124.38, 123.44, 117.57, 117.21, 116.26, 116.11, 115.69, 110.82, 110.40, 109.04; UV-Vis [DMF, λ_{max} (ϵ , $M^{-1} cm^{-1}$)]: 443 nm (90), 318 nm (29875), 307 nm (33370). Molecular mass (m/z): Calcd: 356.25. Found: 379.03 $[M + Na]^+$. Anal. Calcd for $C_{18}H_7F_3N_2O_3$ (%): C, 60.68; H, 1.98; N, 7.86. Found: C, 60.48; H, 2.30; N, 7.86.



2.4. Synthesis of tetra-4-(7-oxochromone phthalocyaninato)Co(II) (CoPc-chr, 3)

A mixture of **1** (0.25 g, 0.867 mM), CoCl₂ (0.0282 g, 0.217 mM), and DBU was heated with stirring in *n*-pentanol (40.0 mL) at 160 °C under nitrogen for 16 h. The reaction mixture was then cooled to room temperature and *n*-hexane was added dropwise to induce precipitation. The precipitate was filtered off using a Millipore filtration setup and then washed with water, MeOH, ethanol (EtOH), DCM, and CH₃CN. The desired product was thereafter recovered via column chromatography using a 50 : 1 CHCl₃ : MeOH solvent system. Yield: 51%; FT-IR ($\nu_{\max}/\text{cm}^{-1}$): $\nu(\text{C}=\text{O})$ 1645, $\nu(\text{C}=\text{N})$ 1592, $\nu(\text{C}-\text{O}-\text{C})$ 1073, 1131; UV-Vis (DMF, λ_{\max} (ϵ , $\text{M}^{-1} \text{cm}^{-1}$)): 679 nm (23075), 343 nm (29176). Molecular mass (m/z): Calcd: 1211.15. Found: 1211.21 [M]⁺, 1212.22 [M + H]⁺, 1213.22 [M + 2H]⁺. Anal. Calcd for CoC₇₂H₂₈F₁₂N₈O₁₂ (%): C, 67.39; H, 2.66; N, 9.25. Found: C, 66.95; H, 2.91; N, 8.97.

2.5. Synthesis of tetra-4-(7-oxy-4-trifluoromethylcoumarin phthalocyaninato)Fe(II) (FePc-cou, 4)

The cyclotetramerization of **2** (0.250 g, 0.702 mM) and FeCl₂·4H₂O (0.0349 g, 0.175 mM) was carried out under the same conditions as reported for **3**. The reaction mixture was allowed to cool to room temperature and *n*-hexane was added dropwise to induce precipitation. The precipitate was filtered using a Millipore filtration setup and then washed with water, MeOH, EtOH, CH₃CN, and diethyl ether. The compound was purified by column chromatography using a 50 : 1 ($v : v$) CHCl₃ : MeOH solvent system. FTIR ($\nu_{\max}/\text{cm}^{-1}$): $\nu(\text{C}=\text{O})$ 1747, $\nu(\text{C}=\text{N})$ 1605, $\nu(\text{C}-\text{O}-\text{C})$ 997, 1122. Yield: 55%; UV-Vis [DMF, λ_{\max} (ϵ , $\text{M}^{-1} \text{cm}^{-1}$)]: 657 nm (16891), 423 nm (17660), 328 nm (81208). Molecular mass (m/z): Calcd: 1480.10. Found: 1480.19 [M]⁺, 1481.22 [M + H]⁺, 1482.21 [M + 2H]⁺. Anal. Calcd for FeC₇₂H₂₈F₁₂N₈O₁₂ (%): C, 58.40; H, 1.91; N, 7.57. Found: C, 57.98; H, 2.15; N, 7.22.

2.6. Synthesis of tetra-4-(7-oxy-4-trifluoromethylcoumarin phthalocyaninato)Co(II) (CoPc-cou, 5)

5 was formulated from the reaction of CoCl₂ (0.0228 g, 0.175 mM) with **2** (0.250 g, 0.702 mM) using the same reaction conditions as specified in the isolation of the aforementioned MPcs. The reaction mixture was cooled to room temperature and *n*-hexane was added dropwise to induce precipitation. The precipitate was filtered using a Millipore filtration setup and then washed with water, MeOH, EtOH, CH₃CN, hexane, and diethyl ether. The compound was further purified by column chromatography using a 1 : 50 ($v : v$) THF : CHCl₃ solvent system. FTIR ($\nu_{\max}/\text{cm}^{-1}$): $\nu(\text{C}=\text{O})$ 1746, $\nu(\text{C}=\text{N})$ 1605, $\nu(\text{C}-\text{O}-\text{C})$ 997, 1122. Yield: 58%; UV-Vis (DMF, λ_{\max} (ϵ , $\text{M}^{-1} \text{cm}^{-1}$)): 669 nm (37422), 331 nm (41139), 283 nm (45899). Molecular mass (m/z): Calcd: 1483.10. Found: 1483.09 [M]⁺, 1484.08 [M + H]⁺, 1485.07 [M + 2H]⁺, 1486.10 [M + 3H]⁺. Anal. Calcd for CoC₇₂H₂₈F₁₂N₈O₁₂ (%): C, 58.27; H, 1.90; N, 7.55. Found: C, 57.92; H, 2.10; N, 7.12.

2.7. X-ray diffraction

The X-ray data for **1** were recorded on a Bruker Apex Duo equipped with an Oxford Instruments Cryojet operating at 100(2) K and an Incoatec microsource operating at 30 W [37]. Crystal and structure refinement data are given in table 1. Selected bond lengths and angles

Table 1. Crystal data and structure refinement data.

Chemical formula	C ₁₇ H ₈ N ₂ O ₃
Formula weight	288.25
Temperature (K)	100(2)
Crystal system	Monoclinic
Space group	<i>P</i> _c
Unit cell dimensions (Å, °)	<i>a</i> = 5.2704(4) <i>b</i> = 14.0315(10) <i>c</i> = 8.9561(6) α = 90.000(5) β = 94.340(4) γ = 90.000(5)
Crystal size (mm)	0.60 × 0.14 × 0.09
<i>V</i> (Å ³)	660.42(8)
<i>Z</i>	2
Density (calc.) (Mg m ⁻³)	1.450
Absorption coefficient (mm ⁻¹)	0.102
<i>F</i> (0 0 0)	296
θ range for data collection (°)	1.5; 26.1
Index ranges	-6 ≤ <i>h</i> ≤ 5 -17 ≤ <i>k</i> < 16 -10 ≤ <i>l</i> ≤ 11
Reflections measured	5668
Observed reflections [<i>I</i> > 2σ(<i>I</i>)]	1284
Independent reflections	1306
Data/restraints/parameters	1306/2/199
Goodness of fit on <i>F</i> ²	1.115
Observed <i>R</i> , <i>wR</i> ²	0.0268; 0.0716
<i>R</i> _{int}	0.022

are given in table 2. The data were collected with Mo-K α ($\lambda = 0.71073$ Å) radiation at a crystal-to-detector distance of 50 mm. The following conditions were used for data collection: omega and phi scans with exposures taken at 30 W X-ray power and 0.50° frame widths using APEX2 [37]. The data were reduced with the program SAINT [38] using outlier rejection, scan speed scaling, as well as standard Lorentz and polarization correction factors. A SADABS semi-empirical multi-scan absorption correction [39] was applied to the data. Direct methods, SHELXS-97 [40], and WinGX [41] were used to solve the structure. All non-hydrogen atoms were located in the difference density map and refined anisotropically with SHELXL-97 [40].

Table 2. Selected bond lengths [Å] and angles [°] for 1.

C6–O2	1.357(3)
C7–O2	1.374(3)
C9–O3	1.396(2)
C10–O3	1.372(3)
C4–O1	1.238(2)
C1–C9	1.403(3)
C12–C13	1.402(3)
C9–O3–C10	118.9(2)
C6–O2–C7	117.9(2)

3. Results and discussion

3.1. Synthesis and characterization

Benzopyrone-derivatized phthalonitriles **1** and **2** were formed via base catalyzed nucleophilic substitution reactions of 4-nitrophthalonitrile with 7-hydroxychromone and 7-hydroxy-4-trifluoromethylcoumarin, respectively (refer to scheme 1). Spectral characterization of **1** and **2** unequivocally confirmed covalent linking of the individual benzopyrone moieties to the phthalonitrile groups, e.g. the FTIR spectral analysis of **1** indicated an absence of the NO₂ vibrational band (which appeared at 1535 cm⁻¹ in the FTIR spectrum of 4-nitrophthalonitrile) and the presence of intense C=O (at 1644 cm⁻¹) and C≡N (at 2231 cm⁻¹) bands, see figures S1–S9 (see online supplemental material at <http://dx.doi.org/10.1080/00958972.2015.1023196>). The ¹H NMR spectra of the ligands showed well-resolved peaks in the region of 7.0–9.0 ppm as is expected for ligands with delocalized π-aromatic systems. The proton signals for both compounds integrate to one as expected and the proton NMR assignments were well supported by ¹³C and cosy NMR spectroscopy.

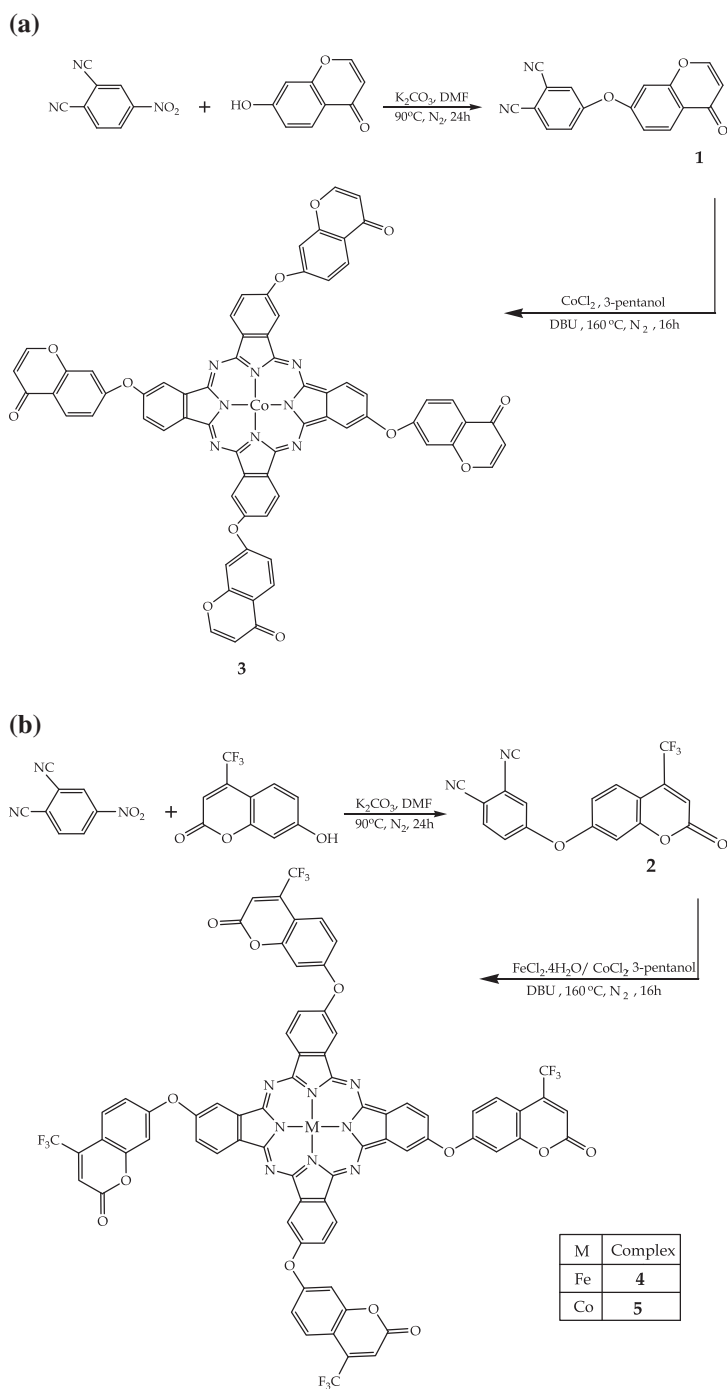
X-ray analysis of **1** revealed that it crystallizes out in a *P*_c space group with two molecules occupying a monoclinic unit cell. The crystal lattice is stabilized by interactions between co-planar chromone moieties of adjacent molecules with interplanar spacings of 4.120 and 4.885 Å, respectively, see figure S10. These intermolecular interactions ultimately lead to columns of molecules of **1** aligned parallel to the [*a*]- and [*b*]-axes.

The aliphatic ether bond angle [C9–O3–C10] of 118.9(2)° results in the chromone moiety not lying in the same plane (deviating by 74.51°) as the phthalonitrile moiety, see figure 1. As expected, the bond angle of the cyclic ether [C6–O2–C7 = 117.9(2)°] is more constrained than the aliphatic ether, but the C–O bond distances for the cyclic ether [C6–O2 = 1.357(3) Å, C7–O2 = 1.374(3) Å] and aliphatic ether [C9–O3 = 1.396(2) Å, C10–O3 = 1.372(3) Å] are still comparable. However, the C–O bond orders of the ethers and carbonyl group [C4–O1 = 1.238(2) Å] are readily distinguishable based on the difference in their bond lengths. The nearly equidistant C≡N bonds are comparable to analogous bond distances of other 4-substituted phthalonitriles [41, 42]. Furthermore, the localized C1–C9 [1.403(3) Å] double bond remains intact as it is similar to the delocalized C–C (e.g. C12–C13 = 1.402(3) Å) bonds found within **1**.

Template cyclotetramerization of **1** and **2** in the presence of a catalyst, DBU, and the desired metal salt (CoCl₂ for **3** and **5** and FeCl₂·4H₂O for **4**) afforded the corresponding MPcs, refer to scheme 1. Complexes **4** and **5** are soluble even in low-boiling organic solvents, including THF, CHCl₃, and DCM, while **3** is only soluble in DMF and DMSO. It is well documented that bulky or long-chain peripheral substituents improve the solubility of MPcs in organic solvents, [43] and thus, as expected, **4** and **5** containing bulky trifluoromethyl groups show enhanced solubilities as compared to **3**.

The absence of medium intensity nitrile stretches found at 2231 cm⁻¹ (for **1**) and 2235 cm⁻¹ (for **2**) in the FTIR spectra of the MPcs is typical of cyclotetramerization (see figures S6–S8). The formation of macrocyclic ring systems is also supported by the observation of strong vibrational bands, ascribed to ν(C=N) at 1592 cm⁻¹ (for **3**) and 1605 cm⁻¹ (for **4** and **5**). Commonality in some of the FTIR bands is also observed between the ligands and their respective MPcs, an example being the ether functional group which vibrates virtually at the same frequency for both.

ESI-TOF mass spectrometry and elemental analysis provided definitive structural characterization for the ligands and their metal complexes. All molecular and cluster ion peaks



Scheme 1. Synthetic pathways for the respective MPCs: (a) tetra-4-(7-oxochromone phthalocyaninato)Co(II) (CoPc-chr, **3**), (b) tetra-4-(7-oxy-4-trifluoromethylcoumarin phthalocyaninato)Fe(II) (FePc-cou, **4**), and tetra-4-(7-oxy-4-trifluoromethylcoumarin phthalocyaninato)Co(II) (CoPc-cou, **5**).

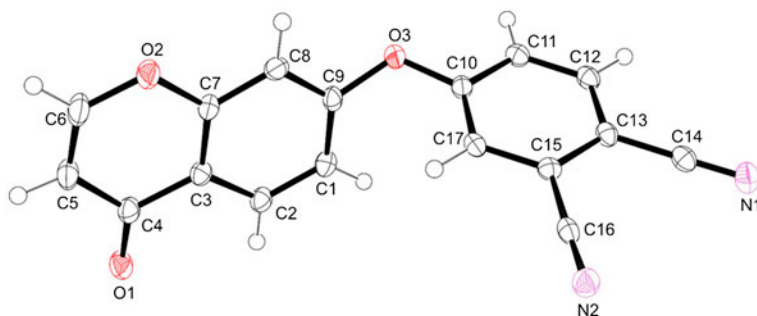


Figure 1. An ORTEP view of **1** showing 50% probability displacement ellipsoids and atom labeling.

were in accord with the calculated m/z values. The mass spectra of the MPcs showed $[M]^+$ ion peaks at m/z values of 1211.21 for **3**, 1480.19 for **4**, and 1483.07 for **5**, respectively, in addition to the protonation molecular ion peaks of the form: $[M + H]^+$, $[M + 2H]^+$, and $[M + 3H]^+$ (for **5** only), see figure S11.

The electronic transitions observed within the UV–Vis spectra of the respective metal complexes (**3–5**) in DMF are in accord with literature trends, see figure 2 [12]. More specifically, the formulated MPcs showed Q - and B -bands in the regions of 600–700 nm and 300–400 nm, respectively (refer to table 3). All three complexes contain a common electron-donating oxy group on their Pc cores; however, **4** and **5** contain the strongly electron-withdrawing trifluoromethyl groups, which lead to blue-shifting of their electronic transitions relative to the corresponding electronic transitions of **3**. The bands at 423 nm for **4** and 283 nm for **5** are ascribed to electronic transitions associated with the highly π -conjugated oxy-coumarin substituents as similar bands occur in the UV–Vis spectrum of **2** at 307 and 443 nm, respectively. Aggregation in MPcs is epitomized by a broadened or split Q -band. Splitting of the Q -band of **4** is indicative of aggregation occurring within

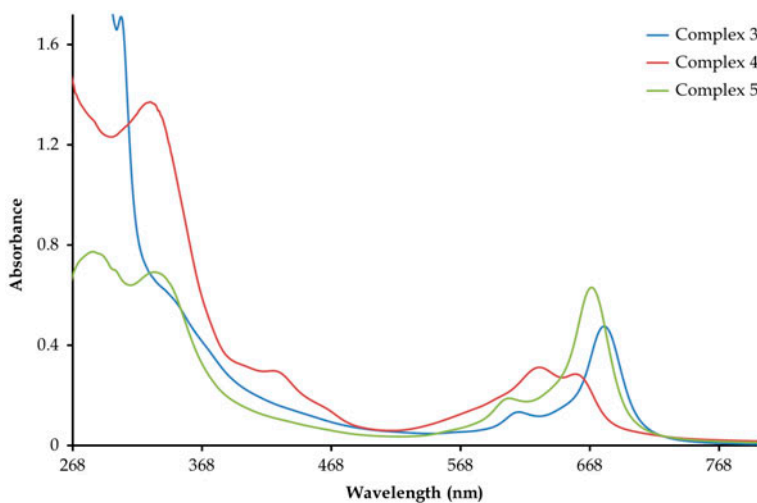


Figure 2. Overlay UV–Vis spectra of **3**, **4**, and **5** at concentrations of 1 mM.

Table 3. UV–Vis absorption wavelengths for 3–5.

Complex	Q-band (nm)	B-band (nm)
3	679	343
4	657 (632)	328
5	669	331

Note: The value in parenthesis is for the aggregate.

solution with the band at higher wavelengths due to the monomer (at 657 nm) and the one at lower wavelengths (at 632 nm) due to the aggregate [44].

3.2. Voltammetry and spectroelectrochemistry

The solution redox properties of the metal complexes were probed via CV and square-wave voltammograms (SWVs) in dried DMF. The MPcs exhibited similar redox behavior with four distinct redox processes observed in their respective CVs and SWVs, see figures 3, S12, and S13. The redox processes denoted as **I**, **II**, and **III** are quasi-reversible as their ΔE values are larger than 103 mV (ΔE value for the standard, ferrocene at 200 mV s⁻¹), indicating slower electron transfer kinetics compared to the standard [44–46]. These redox processes are ascribed to Pc⁻²/Pc⁻³ reduction, M²⁺/M⁺ reduction, and M²⁺/M³⁺ oxidation, while the irreversible redox process denoted as **IV** is due to Pc⁻²/Pc⁻¹ oxidation and the remaining peaks are attributed to aggregation. These assignments are based on comparable redox potentials observed for CoPcs containing coumarin-derived substituents (refer to table 4) [44, 47–49]. Aggregation also resulted in broadened redox couples for couple **III**, while **3** also displays distinct splitting in both the forward and reverse signals, see figure S12. Aggregation phenomena were also common to the β -tetra[7-oxo-4-(methoxyphenyl)-8-methylcoumarin] (oxpcou) CoPc for which broadened redox processes and split *Q*-bands were observed in its CV and UV–Vis spectrum, respectively [46]. Despite the influence of aggregation on the voltammograms, the plots of peak current against square root of scan rate for each complex displayed linear relationships indicating that the redox couples are all diffusion controlled, see figure S14 for the incrementing scan rates of 4.

Spectroelectrochemical experiments were conducted on the MPcs to verify the voltammetric assignments. The UV–Vis spectral changes of the CoPcs (**3** and **5**) are similar, thus, only the spectroelectrochemical data of **4** and **5** will be discussed, see figure 4(A)–(D). Differences in the starting spectra as compared to the original UV–Vis spectrum (see figure 1) are accounted for by the extent of aggregation as a result of varying concentrations of the aggregate and monomer as well as the presence of supporting electrolyte [50].

Investigating the first reduction (denoted as redox couple **II**), the UV–Vis spectral changes of **5** indicate that significant disaggregation occurs resulting in the formation of a well-defined monomeric and red-shifted *Q*-band at 703 nm, see figure 4(A). The aforementioned UV–Vis spectral changes are accompanied by the formation of a new charge transfer band found at 473 nm. It is well documented that red-shifting of the *Q*-band and a new peak forming at around 480 nm is typical of Co^I species [51], hence the redox couple **II** assigned to Co^{II}Pc⁻²/Co^IPc⁻² is confirmed. Furthermore, the presence of diffuse isosbestic points (at 389, 554, and 679 nm) is characteristic of mixed valence species in solution. Nearly 80% regeneration of the initial CoPc was achieved when a zero voltage was applied.

Upon application of negative overpotentials relative to the redox couple **I**, the *Q*- and *B*-bands decrease and a shift of the charge transfer band to a higher wavelength (at 493 nm)

is observed, see figure 4(B). This redox behavior is typical of Pc^{-2} reduction and the formation of Pc^{-3} species [52], thereby confirming that these UV-Vis spectral changes are associated with the $\text{Co}^{\text{I}}\text{Pc}^{-2}/\text{Co}^{\text{I}}\text{Pc}^{-3}$ redox couple.

Thereafter, new sample was injected into the OTTLE cell to investigate the nature of the redox couples within a positive potential window. Examining the UV-Vis spectral changes of redox couple **III**, considerable disaggregation occurs leading to an increase in the intensity of the Q -band, indicative of metal oxidation within a $\text{Co}^{\text{II}}\text{Pc}$ core [53], see figure 4(C). Hence, the voltammetric assignment of redox couple **III** (ascribed to the $\text{Co}^{\text{II}}\text{Pc}^{-2}/\text{Co}^{\text{III}}\text{Pc}^{-2}$ redox process) is corroborated by the attained spectroelectrochemical data. The characteristic

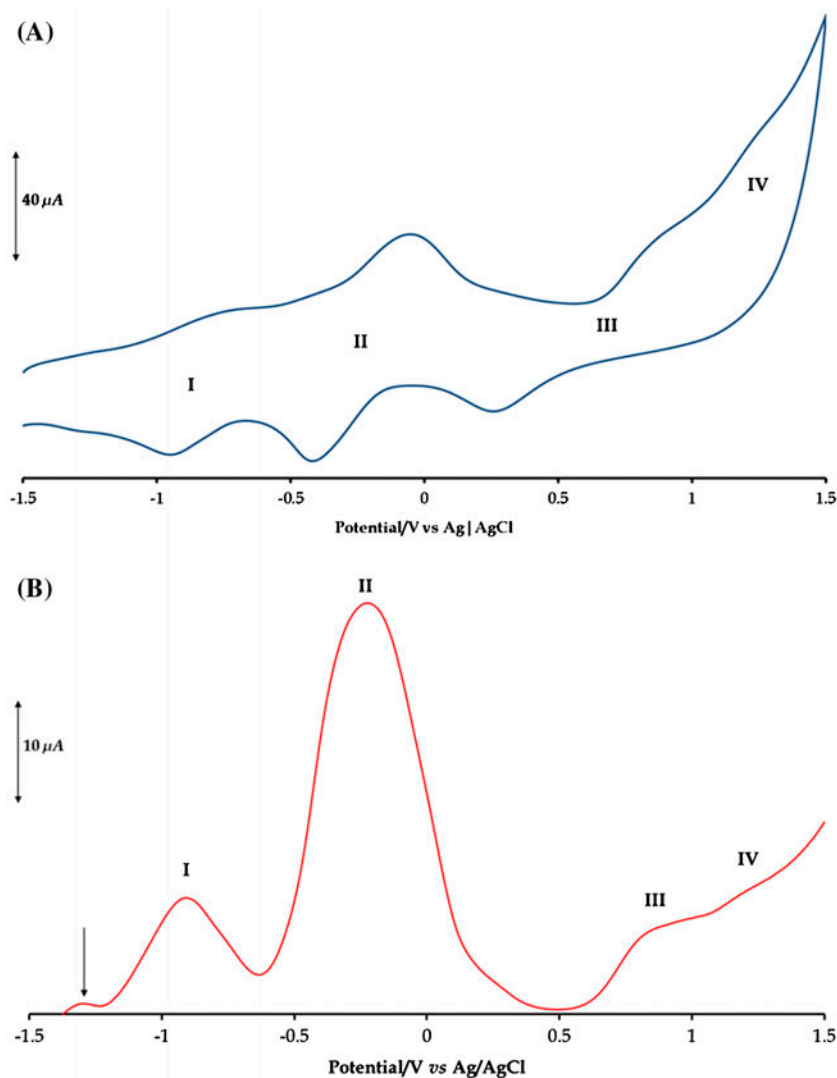


Figure 3. (A) CV and (B) SWV of **4** at 200 mV s^{-1} . The arrow in the SWV indicates a peak associated with aggregation.

Table 4. Comparison of the voltammetric data (in V) between the MPcs **3–5** and reported CoPcs with various tetra-substituted coumarin derivatives.

	M ^I Pc ⁻² /M ^I Pc ⁻³ I	M ^{II} Pc ⁻² /M ^I Pc ⁻² II	M ^{II} Pc ⁻² /M ^{III} Pc ⁻² III	M ^{III} Pc ⁻² /M ^{III} Pc ⁻¹ IV
3	-1.11 ^a	-0.44 ^a	0.40 ^a	1.03 ^b
4	-0.84 ^a	-0.24 ^a	0.55 ^a	1.23 ^b
5	-1.00 ^a	-0.46 ^a	0.42 ^a	1.08 ^b
(β)-CoPc- <i>cfcou</i>	-0.81	-0.47	0.48	0.91
(α)-CoPc- <i>cfcou</i>	-0.86	-0.35	0.42	1.00
CoPc- <i>oxpcou</i>	-1.24	-0.31	0.35	–

Note: *cfcou* = 7-oxo-3-(2-chloro-4-fluorophenyl)coumarin.

$${}^a E_{1/2} = \frac{E_{pa} + E_{pc}}{2}$$

$${}^b E_{pa}$$

increase in the *Q*-band is accompanied by the disappearance of the electronic transition associated with the aggregate and a decrease of the *B*-band leading to well-defined isosbestic points at 349, 474, and 651 nm. Upon applying positive overpotentials relative to redox couple **IV**, the *Q*- and *B*-bands decrease significantly, indicating Pc⁻² oxidation thus confirming the assignment of the redox couple **IV** to Co^{III}Pc⁻²/Co^{III}Pc⁻¹, see figure 4(D) [54].

Compound **4** was also subjected to spectroelectrochemical experiments to validate its voltammetric assignments, see figure S15. Similar to CoPcs **3** and **5**, the UV–Vis spectral behavior for the metal-based reduction of **4** shows a red-shift in the *Q*-band from 657 nm to 663 nm. Subsequently, this leads to significant disaggregation justified by the progressive

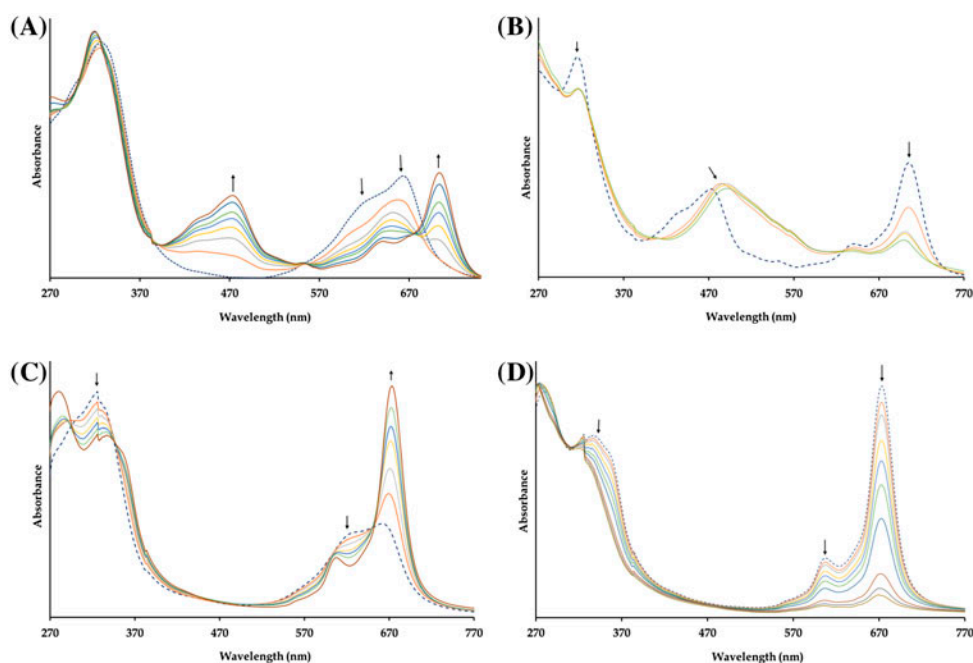


Figure 4. UV–Vis spectral changes of **5** at overpotentials applied at (A) -0.25 V, (B) -1.30 V, (C) 0.78 V, and (D) 1.06 V. The initial spectrum is a dashed line.

decrease in the intensity of the aggregate peak (at 633 nm). It is well documented that a shift in the position of the *Q*-band indicates metal-based electron transfer [55, 56], thereby confirming that redox couple **II** is due to $\text{Fe}^{\text{II}}\text{Pc}^{-2}/\text{Fe}^{\text{I}}\text{Pc}^{-2}$.

Application of negative over potentials relative to redox couple **I** ($E_{1/2} = -1.00$ V) resulted in a decrease in the intensity of its *Q*- and *B*-bands as well as formation of a charge transfer band in the 500–600 nm region. These changes are consistent with ring reduction [56], hence couple **I** is assigned to $\text{Fe}^{\text{I}}\text{Pc}^{-2}/\text{Fe}^{\text{I}}\text{Pc}^{-3}$.

Investigating redox couple **III**, coalescence of the *Q*-bands associated with the monomeric and aggregated species into a single-broad *Q*-band indicates that the resultant $\text{Fe}^{\text{III}}\text{Pc}^{-2}$ species are aggregated. Furthermore, blue-shifting of the monomeric *Q*-band is indicative of metal-based oxidative process associated with the $\text{Fe}^{\text{II}}\text{Pc}^{-2}/\text{Fe}^{\text{III}}\text{Pc}^{-2}$ redox couple. Upon application of a overpotential of 1.22 V, the *Q*- and *B*-bands disappeared, typical of ring oxidation (for the couple $\text{Fe}^{\text{III}}\text{Pc}^{-2}/\text{Fe}^{\text{III}}\text{Pc}^{-1}$) and subsequent Pc decomposition [57].

3.3. Electropolymerization and electrocatalysis

Complexes **3–5** were deposited on Pt working electrodes via electropolymerization. Figures 5, S16, and S17 show evolution of the CVs over 20 repetitive scans at 100 mV s^{-1} . The general increase in currents and shift of peak potentials is typical of electropolymerization of MPCs on electrode surfaces [58, 59]. For **5** (see figure 5), intensification of the peaks associated with the aggregate is observed and ascribed to the progressive elongation of the polymer chain on the Pt electrode surface. The new peak which forms near 0.4 V displays a concomitant increase in intensity as well as a shift to more positive potentials and is ascribed to the electropolymerized MPC. The shift to

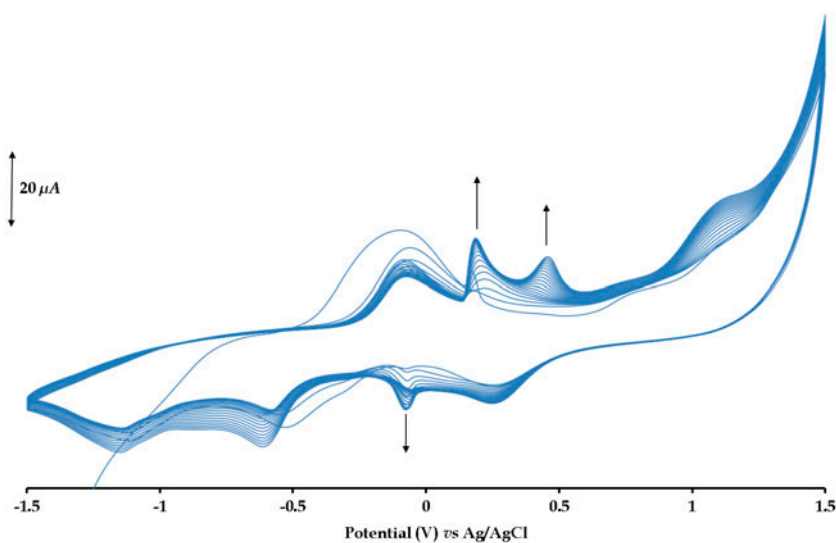


Figure 5. Electropolymerization of **5** at 100 mV s^{-1} for 20 scans. The arrows indicate the progressive increase in the peaks of the aggregate and the formation of a new peak.

positive potentials implies an increase in the electrical resistance of the polymer film, necessitating a larger overpotential to overcome the current inhibition [60].

To confirm modification of the respective working electrode (viz. **3**-Pt, **4**-Pt and **5**-Pt), CVs at incrementing scan rates were run in a pH 7 buffer solution; see figures 6, S18, and S19. The motivation behind the use of a neutral pH stems from the fact that the disproportionation of nitrite to NO is insignificant at this pH. The CVs of the respective modified electrodes (viz. **3**-Pt, **4**-Pt and **5**-Pt) in a pH 7 buffer revealed the presence of the distinctive redox couple **II** (for $\text{Co}^{\text{II}}/\text{Co}^{\text{I}}$) in the negative potential window. In addition, the **3**-Pt- and **5**-Pt-modified working electrodes showed sharp peaks which are similar to the aggregate peaks observed upon polymerization of the respective MPcs. Commonality between the modified working electrodes (**3**-Pt and **5**-Pt) is also observed with the appearance of irreversible metal oxidation peaks (for $\text{Co}^{\text{II}}/\text{Co}^{\text{III}}$) found at positive potentials.

Confirmation of electrode modification is ascertained from the fact that the degree of ion permeability for each modified working electrode is different from each other and the standard (ferrocene) as can be seen by their peak to peak separations (ΔE): 120 mV for **3**-Pt, 290 mV for **4**-Pt, 510 mV for **5**-Pt, and 103 mV for the bare Pt electrode, see figure 7. The surface coverages of the respective modified platinum working electrodes were calculated using the following equation [61]:

$$I_p = \frac{n^2 F^2 A \Gamma(v)}{4RT} \quad (1)$$

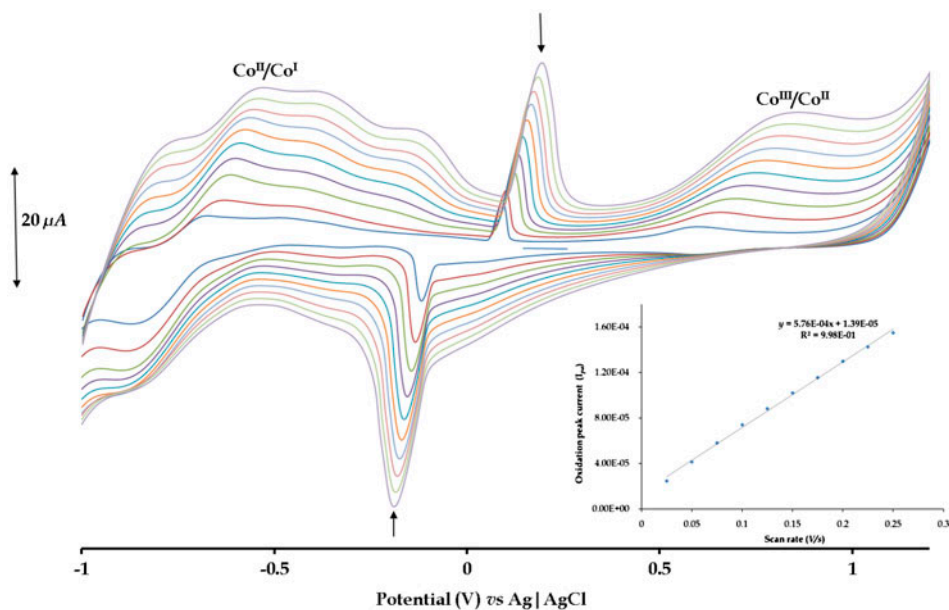


Figure 6. Overlay CVs at incrementing scan rates of **5**-Pt in pH 7.4 buffer solution. Inset: The linear relationship between oxidation peak currents (I_{pa}) vs. scan rates measured at the redox couple **II**. The arrows indicate the peaks associated with the aggregate.

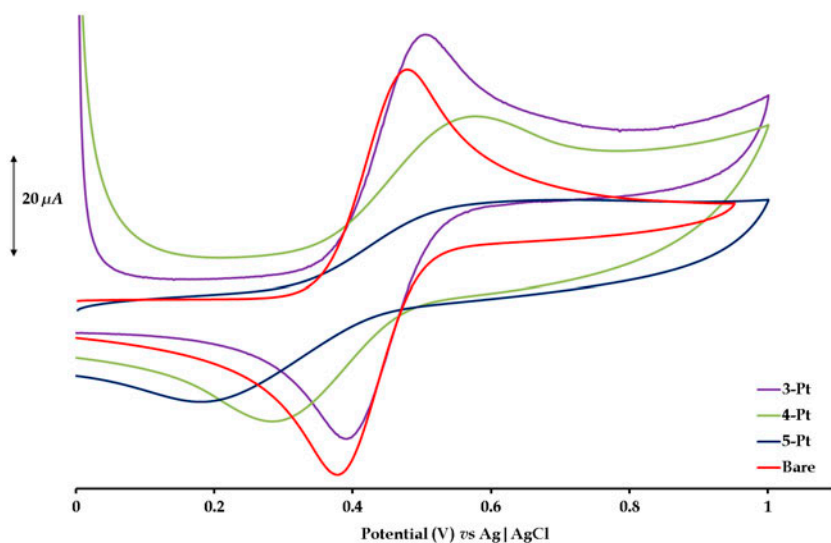


Figure 7. Overlay CVs in 1 mM ferrocene using the bare, 3-Pt, 4-Pt, and 5-Pt working electrodes at 100 mV s^{-1} .

where I_p is the peak current of redox couple **II**, n is the number of electrons, and A is the real surface area (0.132 cm^2) of the bare platinum electrode. A correlation between the surface coverages and the electrocatalytic activities of the modified electrodes indicates that a higher surface coverage ($3.34 \times 10^{-8} \text{ M cm}^{-2}$ for 3-Pt, $2.64 \times 10^{-8} \text{ M cm}^{-2}$ for 4-Pt, and $1.87 \times 10^{-8} \text{ M cm}^{-2}$ for 5-Pt) resulted in a lower electrocatalytic oxidation potential of nitrite (0.75 V for 3-Pt, 0.77 V for 4-Pt and 0.78 V for 5-Pt), see figure 8.

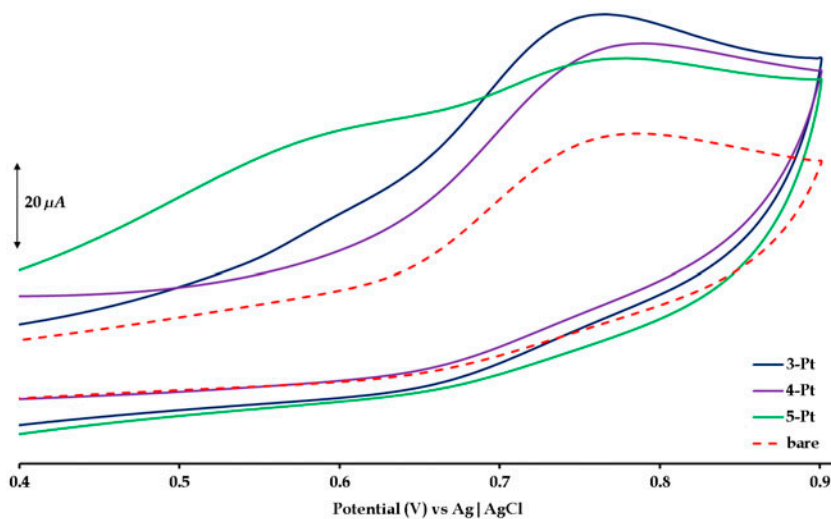


Figure 8. Electrocatalytic oxidation of 1 mM nitrite ion in pH 7.4 buffer solution at 100 mV s^{-1} using the bare and modified working electrodes.

The surface coverage values of the modified electrodes are higher than typical surface coverage values obtained for a monolayer deposited flat on an electrode surface ($1 \times 10^{-10} \text{ M cm}^{-2}$) [62], which is suggestive of electropolymerization. In conjunction with the lowering of the oxidation potentials of nitrite, larger oxidation currents were observed for the modified electrodes as compared to the bare platinum electrode (peak at 0.79 V). The larger current for the modified electrodes is promoted by the metal oxidation couple (i.e. $\text{Co}^{\text{III}}/\text{Co}^{\text{II}}$), which is found in the same vicinity as the electrocatalytic potentials of nitrite using the respective modified electrodes. A linear relationship was established between the oxidation peak currents (I_{pa}) and the square root of the scan rates ($v^{1/2}$) for the oxidation peak potentials which affirms diffusion-controlled behavior. To gain more insight into the mechanism of electrocatalytic oxidation of nitrite, the Tafel slopes were calculated using equation (2):

$$E_p = \frac{2.3RT}{2(1-\alpha)Fn_\alpha} \log v + K \quad (2)$$

where α is the transfer coefficient, v is the scan rate, n_α is the number of electrons in the rate-determining step, and K is the intercept. Tafel slopes were obtained from plots of E_p versus $\log v$, see figure 9. The large Tafel slope of $279 \text{ mV decade}^{-1}$ for 4-Pt in comparison with 3-Pt ($116 \text{ mV decade}^{-1}$) and 5-Pt ($102 \text{ mV decade}^{-1}$) which are in the normal range of $30\text{--}120 \text{ mV decade}^{-1}$, indicates that electrocatalytic oxidation using 4-Pt has no kinetic meaning and is rather suggestive of substrate–catalyst interaction [63]. However, the Tafel slopes of the electropolymerized CoPcs, viz. 3-Pt and 5-Pt are close to $118 \text{ mV decade}^{-1}$, which implies that the first one-electron transfer is rate determining [64].

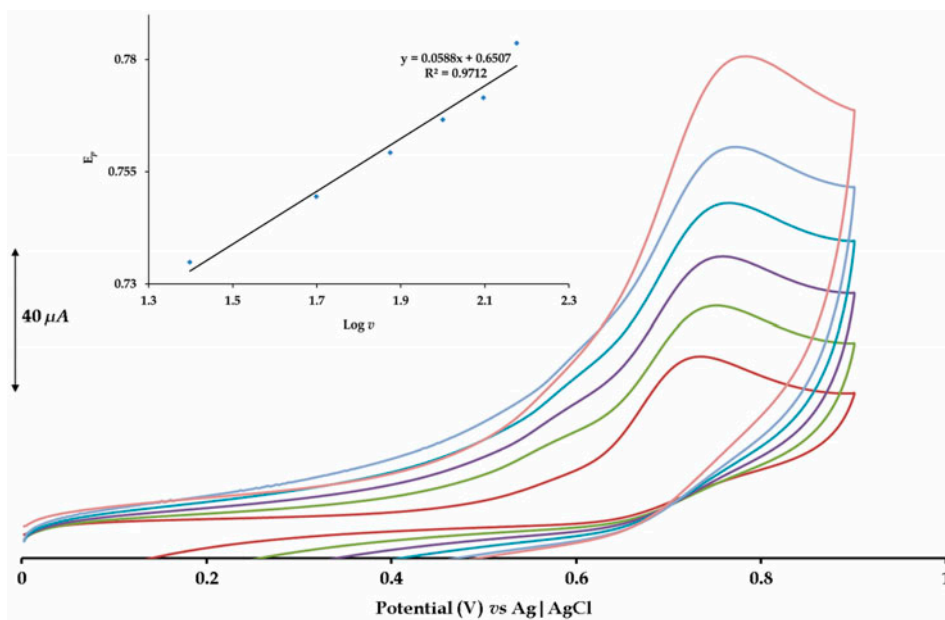


Figure 9. The electrocatalytic oxidation of nitrite (1 mM) using 3-Pt in pH 7 buffer at incrementing scan rate from 75 to 200 mV s^{-1} . Inset: Plot of E_p vs. $\log v$.

4. Conclusion

Co and FePcs bearing chromone and coumarin substituents were synthesized and spectroscopically characterized. The MPcs exhibited similar redox behavior as was deduced from their voltammetric analysis. Voltammetric assignments were well corroborated by UV–Vis spectroelectrochemical data and were comparable to those reported for similar tetra-substituted mononuclear Co and FePcs. Surface modification of bare Pt microelectrodes was achieved readily via electropolymerization (in 20 successive CV cycles). These electropolymerized MPc surfaces acted as electron mediators in electrocatalytic oxidation of nitrite.

Supplementary material

CCDC 1031912 for **1** contains crystallographic data for this article. This data can be obtained free of charge at www.ccdc.cam.ac.uk/conts/retrieving.html [or from the Cambridge Crystallographic Data Center (CCDC), 12 Union Road, Cambridge CB21EZ, UK; Fax: +44(0)1223 336 033; Email: deposit@ccdc.cam.ac.uk]. Supplementary figures S1–S19 associated with this article can be found in the online version.

Acknowledgements

We are grateful to the University of KwaZulu-Natal and the National Research Foundation of South Africa for financial support.

Disclosure statement

No potential conflict of interest was reported by the authors.

References

- [1] K.M. Kadish, K.M. Smith, R. Guilard. *The Porphyrin Handbook*, **19**, 105, Academic Press, San Diego, (2003).
- [2] D. Wöhrle, G. Schnurpfeil, S.G. Makarov, A. Kazarin, O.N. Suvorova. *Macroheterocycles*, **5**, 191 (2012).
- [3] H. Çakıcı, A.A. Esenpınar, M. Bulut. *Polyhedron*, **27**, 3625 (2008).
- [4] E.T. Saka, D. Çakır, Z. Bıyıklıoğlu, H. Kantekin. *Dyes Pigm.*, **98**, 255 (2013).
- [5] N. Sekkat, H. van den Bergh, T. Nyokong, N. Lange. *Molecules*, **17**, 98 (2012).
- [6] M. Burghard, M. Schmelzer, S. Roth, P. Haisch, M. Hanack. *Langmuir*, **10**, 4265 (1994).
- [7] S. Yang, L. Fan, S. Yang. *J. Phys. Chem. B*, **107**, 8403 (2003).
- [8] W.J.R. Santos, P.R. Lima, A.A. Tanaka, S.M.C.N. Tanaka, L.T. Kubota. *Food Chem.*, **113**, 1206 (2009).
- [9] J.H. Zagal, S. Griveau, J.F. Silva, T. Nyokong, F. Bedioui. *Coord. Chem. Rev.*, **254**, 2755 (2010).
- [10] I. Booyesen, F. Matemadombo, M. Durmuş, T. Nyokong. *Dyes Pigm.*, **89**, 111 (2011).
- [11] J. Obirai, N.P. Rodrigues, F. Bedioui, T. Nyokong. *J. Porphyrins Phthalocyanines*, **7**, 508 (2003).
- [12] J.H. Zagal, F. Bedioui, J.P. Dodelet (Eds.). *N₄-Macrocyclic Metal Complexes.*, Springer, New York (2006).
- [13] A.I. Adebayo, T. Nyokong. *Polyhedron*, **28**, 2831 (2009).
- [14] B. Çeken, M. Kandaz, A. Koca. *J. Coord. Chem.*, **65**, 3383 (2012).
- [15] S. Seelan, M.S. Agashe, D. Srinivas, S. Sivasanker. *J. Mol. Catal. A: Chem.*, **168**, 61 (2001).
- [16] C. Barrera, I. Zhukov, E. Villagra, F. Bedioui, M.A. Páez, J. Costamagna, J.H. Zagal. *J. Electroanal. Chem.*, **589**, 212 (2006).

- [17] J.C. Obirai, T. Nyokong. *J. Electroanal. Chem.*, **600**, 251 (2007).
- [18] V. Mani, R. Devasenathipathy, S.-M. Chen, S.-T. Huang, V.S. Vasantha. *Enzyme Microb. Technol.*, **66**, 60 (2014).
- [19] B.H. Havsteen. *Pharmacol. Ther.*, **96**, 67 (2002).
- [20] M. Çamur, M. Bulut, M. Kandaz, O. Güney. *Polyhedron*, **28**, 233 (2009).
- [21] S.K. K. Sharma, S. Kumar, K. Chand, A. Kathuria, A. Gupta, R. Jain. *Curr. Med. Chem.*, **18**, 3825 (2011).
- [22] C. Zwergel, S. Valente, A. Salvato, Z. Xu, O. Talhi, A. Mai, A. Silva, L. Altucci, G. Kirsch. *Med. Chem. Commun.*, **4**, 1571 (2013).
- [23] Y. Li, Z. Yang, Z. Liao, Z. Han, Z. Liu. *Inorg. Chem. Commun.*, **13**, 1213 (2010).
- [24] S.H. Kim, Y.H. Lee, S.Y. Jung, H.J. Kim, C. Jin, Y.S. Lee. *Eur. J. Med. Chem.*, **46**, 1721 (2011).
- [25] M.M. Ghoneim, A. Tawfik. *Anal. Chim. Acta*, **511**, 63 (2004).
- [26] M. Camur, M. Bulut. *Dyes Pigm.*, **77**, 165 (2008).
- [27] A.S. Başak, A.R. Özkaya, A. Altındal, B. Salih, A. Şengüld, Ö. Bekaroğlu. *Dalton Trans.*, **43**, 5858 (2014).
- [28] R. Baker, D.P. Wilkinson, J. Zhang. *Electrochim. Acta*, **53**, 6906 (2008).
- [29] S. Nyoni, T. Mugadza, T. Nyokong. *Electrochim. Acta*, **128**, 32 (2014).
- [30] C. Caro, F. Beddioui, J.H. Zagal. *Electrochim. Acta*, **47**, 1489 (2002).
- [31] C.-Y. Lin, A. Balamurugan, Y. Lai, K. Ho. *Talanta*, **82**, 1905 (2010).
- [32] R. Cammack, C.L. Joannou, X.Y. Cui, C.T. Martinez, S.R. Maraj, M.N. Hughes. *Biochim. Biophys. Acta*, **1411**, 475 (1999).
- [33] H. Özena, U. Kamber, M. Karaman, S. Gül, E. Atakis, K. Özcan, O. Atakisi. *Exp. Toxicol. Pathol.*, **66**, 367 (2014).
- [34] A. Cockburn, C.W. Heppner, J.L.C.M. Dorne. *Encycl. Food Saf.*, **2**, 332 (2014).
- [35] H. Zhang, S. Qi, Y. Dong, X. Chen, Y. Xu, Y. Ma, X. Chen. *Food Chem.*, **151**, 429 (2014).
- [36] D. Yu, D. Yong, S. Dong. *J. Environ. Sci.*, **25**, 785 (2013).
- [37] Bruker APEX2. *SAINT and SADABS*. Bruker AXS, Madison, WI (2010).
- [38] R.H. Blessing. *Acta Crystallogr., Sect. A*, **51**, 33 (1995).
- [39] G.M. Sheldrick. *Acta Crystallogr., Sect. A*, **64**, 112 (2008).
- [40] L.J. Farrugia. *J. Appl. Crystallogr.*, **45**, 849 (2012).
- [41] A. Hori, Y. Inoue, H. Yuge. *Acta Crystallogr., Sect. C*, **67**, o154 (2011).
- [42] M. Dinçer, A. Ağar, N. Akdemir, E. Ağar, N. Özdemir. *Acta Crystallogr., Sect. E*, **60**, o79 (2004).
- [43] E. Güzel, A. Atsay, S. Nalbantoglu, N. Şaki, A.L. Dogan, A. Gül, M.B. Koçak. *Dyes Pigm.*, **97**, 238 (2013).
- [44] S. Altun, A.R. Özkaya, M. Bulut. *Polyhedron*, **48**, 31 (2012).
- [45] A. Alemdar, A.R. Özkaya, M. Bulut. *Polyhedron*, **28**, 3788 (2009).
- [46] Z. Odabaş, H. Kara, A.R. Özkaya, M. Bulut. *Polyhedron*, **39**, 38 (2012).
- [47] Y. İpek, H. Dinçer, A. Koca. *Sens. Actuators, B*, **193**, 830 (2014).
- [48] M. Kandaz, M.N. Yarasir, A. Koca. *Polyhedron*, **28**, 257 (2009).
- [49] M. Sevim, M.N. Yaras, A. Koca, M. Kandaz. *Dyes Pigm.*, **111**, 190 (2014).
- [50] A. Erdoğan, I.A. Akinbulu, T. Nyokong. *Polyhedron*, **29**, 2352 (2010).
- [51] A. Erdoğan, I.N. Booyesen, T. Nyokong. *Synth. Met.*, **161**, 241 (2011).
- [52] I.A. Akinbulu, T. Nyokong. *Polyhedron*, **29**, 1257 (2010).
- [53] G. Özgül, A. Taştemel, A.R. Özkaya, M. Bulut. *Polyhedron*, **85**, 181 (2015).
- [54] A. Alemdar, A.R. Özkaya, M. Bulut. *Synth. Met.*, **160**, 1556 (2010).
- [55] M. Arıcı, D. Arıcan, A.L. Uğur, A. Erdoğan, A. Koca. *Electrochim. Acta*, **87**, 554 (2013).
- [56] I. Özçşemeci, A.K. Burat, Y. İpek, A. Koca, Z. Aayır. *Electrochim. Acta*, **89**, 270 (2013).
- [57] B.O. Agboola, K.I. Ozoemena, T. Nyokong. *Electrochim. Acta*, **51**, 4379 (2006).
- [58] V. Çakır, H. Kantekin, Z. Bıyıklıoğlu, A. Koca. *Polyhedron*, **81**, 525 (2014).
- [59] Z. Bıyıklıoğlu, V. Çakır, F. Demir, A. Koca. *Synth. Met.*, **196**, 166 (2014).
- [60] B.O. Agboola, K.I. Ozoemena, T. Nyokong. *Electrochim. Acta*, **51**, 6470 (2006).
- [61] A. Maringa, E. Antunes, T. Nyokong. *Electrochim. Acta*, **121**, 93 (2014).
- [62] F. Matemadombo, T. Nyokong. *Electrochim. Acta*, **52**, 6856 (2007).
- [63] F. Bedioui, S. Griveau, T. Nyokong, A. John Appleby, C.A. Caro, M. Gulppi, G. Ochoa, J.H. Zagal. *Phys. Chem. Chem. Phys.*, **9**, 3383 (2007).
- [64] N. Nombona, P. Tau, N. Sehlotho, T. Nyokong. *Electrochim. Acta*, **53**, 3139 (2008).